Numerical study of the influence of picosecond laser spot size on ablated depth and threshold fluence of metal

Yiming Zhang[*a,b], Benjamin Lauer[a], Beat Neuenschwander[a], Valerio Romano[a,b]
[a]Institute of Applied Laser, Photonics and Surface Technologies, Bern University of Applied Science, Pestalozzistrasse 20, 3400 Burgdorf, Switzerland; [b]Institute of Applied Physics, University of Bern, Sidlerstrasse 5, 3012 Bern, Switzerland

ABSTRACT

Picosecond laser systems have been widely used in industrial microprocessing applications since they are a cost-effective tool to achieve high throughput. To better understand the ablation process, firstly the dependence of the ablation depth and the threshold fluence on the laser spot size were determined experimentally by performing ablation with a 10ps pulsed laser system. Further, a 2D axisymmetric model was established to demonstrate the possible mechanism of the phenomena. Three sets of spot radii, namely 15.5µm, 31.5µm and 49.6µm, respectively with equal laser peak fluences ranging from 0.6J/cm^2 to 4.5J/cm^2 were applied on copper. It was found that the laser ablation depth increases while the threshold fluence decreases with decreasing spot size at identical peak fluence. A 2D axisymmetric thermomechanical model was developed to qualitatively illustrate the mechanism behind these phenomena. The numerical results of the position where the tensile stress exceed to ultimate tensile strength (UTS) of copper show the same trend as the experimental ones. The longitudinal tensile stress was seen to play a more crucial role than the radial tensile / compressive stress on laser ablation process. The impact of the thermal stress on the ablation depth and threshold fluence is derived from the lattice temperature gradient along the surface of the material, leading to spallation and possible modifications of the mechanical properties already at lower laser peak fluences. This is elucidated numerically and analytically. The deviation of the experimental results from the simulation might be attributed to the fact that this simulation model is static. Nevertheless, at low laser fluences, this static approach can provide good explanations of the cold ablation with ultrashort pulsed laser. The limitation of this model is also illustrated.

Keywords: Picosecond pulsed laser, laser spot size, thermal stress, temperature gradient

1. INTRODUCTION

Short and ultrashort pulsed laser systems have been widely used in the industrial world as a cost-effective tool for various applications. Laser ablation with picosecond and femtosecond pulsed laser has been studied in the past theoretically and experimentally in order to find the optimized way to increase the processing throughput, which is influenced by many factors, such as pulse duration, pulse shape, beam polarization and ambient gas. Recently ablation experiments at 10 ps pulse length have shown the dependence of ablation depth and threshold fluence on laser spot size [1]. The theoretical study of short and ultrashort pulsed laser and material interaction [2],[3],[21] can be attempted by

* yiming.zhang@bfh.ch; phone +41 (0)34 426 43 59; alps.ti.bfh.ch

Laser Applications in Microelectronic and Optoelectronic Manufacturing (LAMOM) XXI, edited by Beat Neuenschwander, Stephan Roth, Costas P. Grigoropoulos, Tetsuya Makimura, Proc. of SPIE Vol. 9735, 97350M · © 2016 SPIE · CCC code: 0277-786X/16/$18 · doi: 10.1117/12.2210981

applying the two temperature model (TTM), however, there is an obvious limitation given by the non-thermal laser ablation processes, as reported in literature [12],[13]. In addition, the mechanisms of some phenomena such as incubation effect [4],[22], formation of periodical surface pattern [5] are still not clearly interpreted. Therefore a more detailed process description should be obtained by establishing more complete models.

Many efforts have been taken by some researchers beyond the simple determination of temperature distribution. The molecular dynamic (MD) method, combined with TTM, has been employed by some researchers for a couple of decades [6-8]. This method is based on Newton's law, in which the governing equation of lattice subsystem in TTM is fully substituted by MD equation of motion. Therefore the bulk effects, surface effects and other processes taking place on the surface could be described microscopically. The time-consuming calculation due to the inherently higher degree of freedom, however, is the most significant disadvantage of this technique. Recently Particle-in-Cell (PIC) approach [9] was reported to simulate the material damage induced by femtosecond pulsed laser. This method, based on the equation of motion, can directly simulate the formation of the laser induced crater derived from basic physics principles. In addition to these particle based approaches, several developments on the basis of TTM have been made by some other researchers. Ling Zhou et al. [10] established a 1D Dual-Hyperbolic Two Step model for the case of ultra-short pulse laser ablation. Such model is suitable for the situation where the pulse duration of the laser is in the subpicoscond range. J. K. Chen et al. [11] proposed a semi-classical two temperature model which combined the Dual-Hyperbolic two step model and Boltzmann transport equations so that the non-equilibrium effect of electron transport in electron subsystem during the ultra-short pulse laser irradiation can be taken into consideration. Apart from the thermal dynamics simulation, some work explaining "cold ablation" by ultrashort pulsed laser and material interaction has been done by considering the thermomechanical effects. J. K. Chen et al. [12] utilized a set of transient thermoelasticity equations in 1D model to simulate thermal and non-thermal deformation in metal film induced by ultrashort pulsed laser. Recently Yong Gan et al. [13] has applied 1D model combining MD with TTM to investigate the thermomechanical behavior of copper thin film under the irradiation of sub-picosecond laser.

In this work the results of laser ablation experiments with 10 picosecond pulses on copper [1] are shown. They indicate several laser spot size dependent phenomena, including an increase in laser ablation depth, enhanced ablation efficiency and declining threshold fluence with decreasing laser spot size. Since thermal loading caused by short or ultrashort laser pulse can induce significantly high strain rates which can reach the order of magnitude of 10^6 to 10^9 s^{-1}, thermomechanical effects were considered and consequently the TTM was coupled with thermoelasticity theory. This was then developed and expanded into a 2D axisymmetric model. The numerical results compared with experimental ones and the possible mechanism of the dependence of ablation depth and threshold fluence on laser spot size can be explained in terms of thermal stress. Finally the limitation of such model is illustrated.

2. EXPERIMENT

Setup and results

A FUEGO^{TM} (JDSU Ultrafast, former Time Bandwidth Products, Switzerland) ps-laser system working at a wavelength of 1064 nm with pulse duration of about 10 ps was used. Gaussian beam with three different laser spot sizes, w_0 = 15.5 µm, 31.5 µm and 49.6 µm, were obtained and focused on the surface of copper Cu-DHP with various optical

components in this experiment. More details can refer to [1]. The measured ablation depth per pulse by depth method is shown in Figure 1 and deduced threshold fluences are 0.39J/cm^2, 0.566J/cm^2 and 0.567J/cm^2 for the laser spot size of 15.5 μm, 31.5 μm and 49.6 μm, respectively.

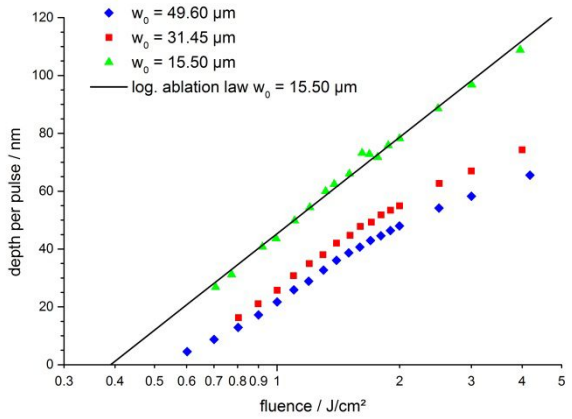

Figure 1 Ablation depth per pulse as a function of fluence for copper

The dependence of ablation depth and threshold fluence on laser spot size was found. Larger ablation depth could be obtained with smaller spot size at identical fluence and threshold fluence decreased as the spot size enlarged. In order to understand mechanism behind such results, the numerical study follows in the next part.

3. 2D AXISYMMETRIC MODEL

3.1 Governing equations

The following governing equations of the model are consisted of two temperature model fully coupled with thermoelasticity theory. Considering the computational efficiency, the 2D axisymmetric model is developed.

$$C_e(T_e)\frac{\partial T_e}{\partial t}+\nabla\cdot(-\kappa_e\nabla T_e)=-G(T_e-T_l)+S(r,z,t) \tag{1}$$

$$C_l(T_l)\frac{\partial T_l}{\partial t}+\nabla\cdot(-\kappa_l\nabla T_l)=G(T_e-T_l)-(3\lambda+2\mu)aT_l\dot{\xi}_{kk} \tag{2}$$

$$\rho\frac{\partial^2 u_r}{\partial t^2}=\mu\nabla^2 u_r+(\lambda+\mu)\frac{\partial}{\partial r}\xi_{kk}-(3\lambda+2\mu)a\frac{\partial}{\partial r}(T_l-T_0)+F_r \tag{3}$$

$$\rho\frac{\partial^2 u_z}{\partial t^2}=\mu\nabla^2 u_z+(\lambda+\mu)\frac{\partial}{\partial z}\xi_{kk}-(3\lambda+2\mu)a\frac{\partial}{\partial z}(T_l-T_0)+F_z \tag{4}$$

Where $C_e(T_e)$ and $C_l(T_l)$ are temperature dependent electron heat capacity and lattice heat capacity, respectively, κ_e is electron thermal conductivity, κ_l is lattice thermal conductivity, G is electron-phonon coupling coefficient,

$\xi_{kk} = \xi_{rr} + \xi_{zz}$ is the sum of principal strains in two directions, λ and μ are Lamé constant and shear modulus respectively, a is linearly thermal expansion coefficient, and F_r and F_z are transversal and longitudinal component of hot-electron blast force, respectively. The thermal source term of Gaussian laser beam is $S(r,z,t) = \alpha^{-1}(1-R)\frac{F_{peak}}{\tau_p}\exp(\frac{r^2}{\omega_0^2})\exp(-\alpha^{-1}z)\sqrt{4\ln 2/\pi}\exp(4\ln 2(\frac{t-2\tau_p}{\tau_p})^2)$, where the absorption coefficient α and reflectivity R , based on critical model of optical property [14], are the function of temperature of both subsystems. The specific expressions of some variables are as follows

$$C_e(T_e) = \begin{cases} C_{e0}T_e & T_e < T_F/\pi^2 \\ 2C_{e0}T_e/3 + C'_e/3 & T_F/\pi^2 \le T_e < 3T_F/\pi^2 \\ Nk_B + C'_e/3 & 3T_F/\pi^2 \le T_e < T_F \\ 3Nk_B/2 & T_e \ge T_F \end{cases},$$

Where $C_{e0} = \frac{1}{2}\frac{\pi^2 k_B N}{T_F}$, $C'_e = C_{e0}T_F/\pi^2 + \frac{3Nk_B/2 - C_{e0}T_F/\pi^2}{T_F - T_F/\pi^2}(T_e - T_F/\pi^2)$

$C_l(T_l) = C_l + L_m D_m + L_v D_v$, where L_m and L_v are latent heat of fusion and evaporation, respectively. The lattice thermal conductivity is taken as 1% of the thermal conductivity of bulk metal, $\kappa_l = 0.01\kappa_0$, since the mechanism of heat conduction in metals is dominated by electrons. [15]

In the higher laser fluence case the electronic thermal conductivity reads [16] $\kappa_e = C\theta_e\frac{(\theta_e^2+0.164)^{5/4}(\theta_e^2+0.44)}{(\theta_e^2+0.092)^{1/2}(\theta_e^2+b\theta_l)}$,

where $\theta_e = \frac{T_e}{T_F}$, $\theta_l = \frac{T_l}{T_F}$

This is valid up to the Fermi temperature, T_F .

The linearly electronic temperature dependent electron-lattice coupling coefficient reads [17] $G = G_0[\frac{A}{B}(T_e + T_l) + 1]$

Lamé constant λ and shear modulus μ could be expressed in terms of Young's modulus E_Y and Poisson ratio γ ,

$\lambda = \gamma E_Y/[(1+\gamma)(1-2\gamma)]$ and $\mu = E_Y/[2(1+\gamma)]$

Considering the hot electron blast force induced by the interaction among electron system in non-thermal equilibrium

state, such volume force reads $\vec{F} = \nabla \cdot \vec{P}$, where $P = \frac{2}{3} C_e(T_e) T_e$ which is the generic form of electron pressure, and holds up to electron temperature $T_e \approx T_F$ [11].

The second term on the right hand side of equation (2) represents the energy gained unit time and unit volume in lattice system, which is induced by considering Helmholtz and Gibbs free energy. To a better understanding of the role of stresses playing in thermoelasticity theory, equation (3) and (4) are expended into the form of matrix

$$\rho \frac{\partial^2 u_r}{\partial t^2} - \nabla \cdot (\mu \begin{Bmatrix} \frac{\partial}{\partial r} u_r \\ \frac{\partial}{\partial z} u_r \end{Bmatrix} + \begin{Bmatrix} \lambda(\frac{\partial u_r}{\partial r} + \frac{\partial u_z}{\partial z}) + \mu \frac{\partial u_r}{\partial r} \\ \mu \frac{\partial}{\partial r} u_z \end{Bmatrix} - \begin{Bmatrix} (3\lambda + 2\mu) a (T_l - T_0) \\ 0 \end{Bmatrix}) = F_r \tag{5}$$

$$\rho \frac{\partial^2 u_z}{\partial t^2} - \nabla \cdot (\mu \begin{Bmatrix} \frac{\partial}{\partial r} u_z \\ \frac{\partial}{\partial z} u_z \end{Bmatrix} + \begin{Bmatrix} \mu \frac{\partial}{\partial z} u_r \\ \lambda(\frac{\partial u_r}{\partial r} + \frac{\partial u_z}{\partial z}) + \mu \frac{\partial u_z}{\partial z} \end{Bmatrix} - \begin{Bmatrix} 0 \\ (3\lambda + 2\mu) a (T_l - T_0) \end{Bmatrix}) = F_z \tag{6}$$

The terms in the bracket on the left hand side of the above two expressions represent the principal and shear stresses along r and z axial, respectively. In 2D symmetric model, the two principal stresses and two shear stresses are

$$\sigma_{rr} = \lambda \xi_{kk} + 2\mu \xi_{rr} - (3\lambda + 2\mu) a (T_l - T_0)$$

$$\sigma_{zz} = \lambda \xi_{kk} + 2\mu \xi_{zz} - (3\lambda + 2\mu) a (T_l - T_0)$$

$$\tau_{rz} = \tau_{zr} = \mu(\frac{\partial u_r}{\partial z} + \frac{\partial u_z}{\partial r})$$

The schematic of these stresses are illustrated in Figure 2.

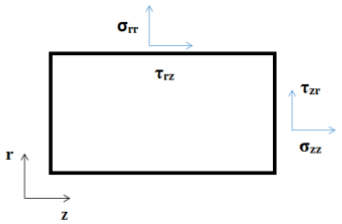

Figure 2 The schematic of illustration of principal and shear stresses

3.2 Boundary conditions and initial values

For the mechanical response, it is assumed that the front and rear surfaces of the bulk are stress free, which means $\sigma_{zz}(0,t) = \sigma_{zz}(d,t) = 0$. This indicates the irradiated surface is free to expand. Both the initial temperatures of electron and lattice subsystems are room temperature $T_0 = 300\,K$.

The parameters used in the model are listed in Table 1 [18-20]

Table 1. The physical properties of copper

Nomenclature and Value			
a	linearly thermal expansion coefficient	$17\times10^{-6}(1/K)$	
A	Coefficient of electron thermal conductivity	$1.28\times10^{7}(1/sK^{2})$	
B	Coefficient of electron thermal conductivity	$1.23\times10^{11}(1/sK^{2})$	
C	Coefficient of electron heat conductivity	$377Wm^{-1}K^{-1}$	
C_l	lattice specific heat capacity	$3.5\times10^{6}(J/m^{3}K)$	
E_Y	Young's modulus	$124GPa$	
G_0	Coupling coefficient of electron and lattice	$10^{16}(J/m^{3}sK)$	
k_B	Boltzmann constant	$1.38\times10^{-23}m^{2}kgs^{-2}k^{-1}$	
k_0	Coefficient of electron thermal conductivity	$400(Jm^{-1}s^{-1}K^{-1})$	
L_m	Latent heat of fusion	$205000(J/kg)$	
L_v	latent heat of vaporization	4796000(J/kg)	
N	Number density of free electron	$8.41\times10^{28}(1/m^{3})$	
T_0	Initial value of temperature	$300K$	
T_F	Fermi temperature	81200K	
Greek symbols			
ρ	Solid density of copper	$8.9g/cm^{3}$	
ρ_L	Liquid density of copper	$8.02g/cm^{3}$	
γ	Poisson ratio	0.34	
Subscripts			
e	Electron	v	vapor
l	lattice	L	liquid

4. RESULTS AND DISCUSSION

The experimental cases with three different laser spot sizes have been simulated with the developed model. The spatial distribution of two principal stresses at different time are shown in Figure 3 and Figure 4. The transition of longitudinal principal stress from compressive stress to tensile stress is clearly shown in all simulated cases. Nonetheless, with the increase of spot size the maximum value of tensile stress decreases and the point where tensile stress exceeds the ultimate tensile strength (UTS) of copper (220MPa) shifts slightly towards the surface of the target. The summary of these results is found in Table 2. Similarly, as shown in Figure 3, the transversal principal stress at the center of irradiated zone also changes from compressive stress to tensile stress as time goes by. And the maximum tensile stress at the center area declines as the spot size enlarges. The oscillation of the curve might be attributed to the coarse mesh along radial direction which is for the purpose of increasing the calculation efficiency. Nonetheless, these results are acceptable since such a transversal stress is not the dominating force that would lead to deformation of the material.

Table 2. The numerical results of maximum tensile stress and depth where the stress exceeds to UTS in Figure 2

Laser Fluence \ Spot Size		15.5 μm	31.5 μm	49.6 μm
1J/cm^2	Maximum tensile stress	310MPa	274.7MPa	270.3MPa
	Depth	68.97nm	64.3nm	64.3nm
2J/cm^2	Maximum tensile stress	1037.4MPa	899MPa	896.7MPa
	Depth	73.3nm	72.5nm	72.2nm

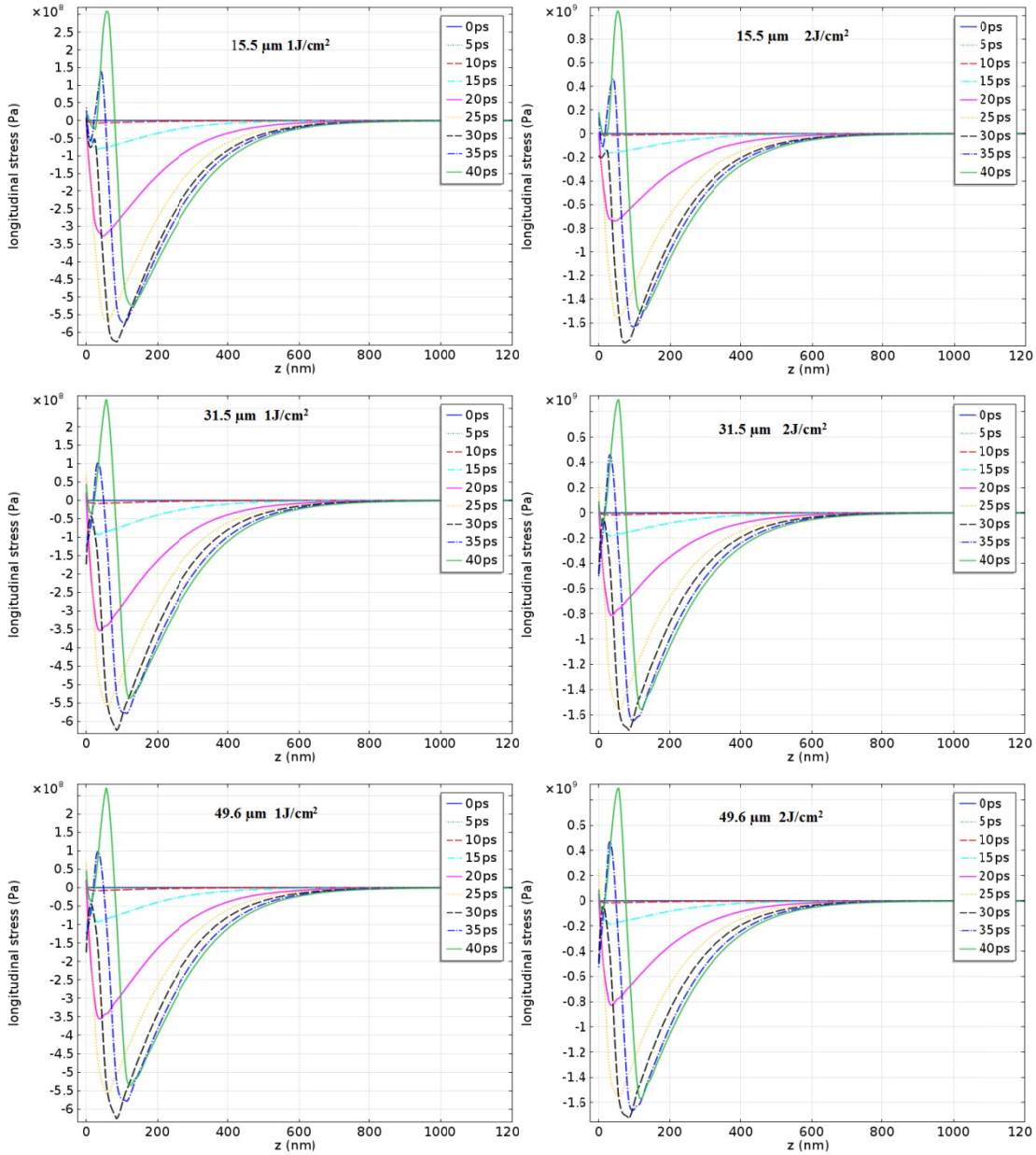

Figure 3 The distribution of longitudinal stress at different time (15.5 μm, 31.5 μm and 49.6 μm, respectively, at fluence of 1J/cm^2 in the left column and 2J/cm^2 in the right column)

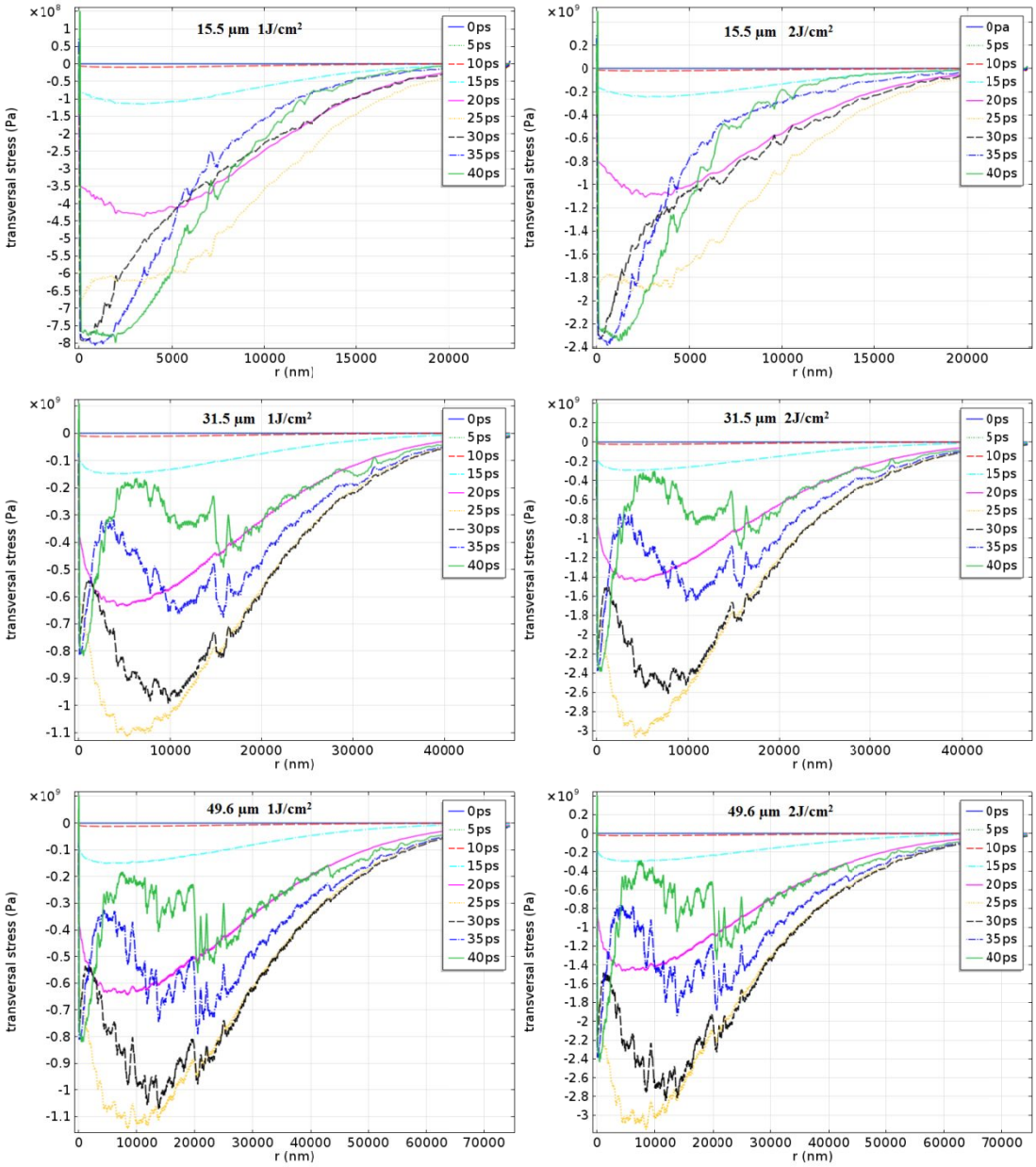

Figure 4 The distribution of transversal stress at different time (15.5 μm, 31.5 μm and 49.6 μm, respectively, at fluence of 1J/cm^2 in the left column and 2J/cm^2 in the right column)

Now, a picture of deformation of metal under low fluences irradiation is clearly formed with the help of laser induced thermal stress along radial and axial directions. Compared with the tensile stresses in both directions, the longitudinal ones are approximately two times larger than the transversal ones. Such stress might be the dominating cause for the

forces that lead to the deformation of the material. At both laser fluence levels, attributed respectively to the increased tensile stress along the axial direction and to the center area in the case of smaller spot size with fixed fluences, the material is more readily deformed. Moreover the calculated maximum tensile stress is larger than the ultimate tensile strength (UTS) of copper (220MPa). Therefore the larger thermal stress induced by smaller spot size could be the possible mechanism of the dependence of threshold fluence on spot size. On the other hand, as the position of tensile stress which exceeds the UTS goes slightly deeper into the material in the case of smaller spot size shown in Table 2, the corresponding ablation depth might increase. Such trend is identical with the experimental results. The reason why the calculated values do not show the same clear difference as the experimental ones is that the deformation assumed in the model is static, while in the experimental reality more complex dynamical deformations occur. Specifically, the laser induced thermal stress in the model can propagate along the longitudinal direction and attenuate spontaneously even if the tensile stress exceeds the UTS. In the experiment, however, once the delamination occurs, there would be a jump of mechanical energy along the detached interface and loss of energy in other forms which could interfere the further propagation and strength of the stress. Therefore the evaluated depth by the model is larger than the experimental one and the difference of these values with various laser spot sizes is no more obvious.

Reviewing the expression for the two principal stresses in part 3, the further analysis of the mechanism of spot size dependent phenomena is provided. As shown both stresses are the function of principal strains in two directions. Furthermore the radial strain reads $\xi_{rr} = \frac{\partial u_r}{\partial r} = \frac{\partial u_r}{\partial T_l}\frac{\partial T_l}{\partial r}$. Based on thermoelasticity theory, $\frac{\partial u_r}{\partial T_l}$ is assumed to be a constant, proportional to linear expansion coefficient a, and approximately $\frac{\partial u_r}{\partial T_l} = aR$ where R is the width of the target. Then radial strain ξ_{rr} just depends on the lattice temperature gradient along surface. As the spot size decreases the lattice temperature gradient along surface would become sharper. Hence the correspondingly increased ξ_{rr} would lead to a larger longitudinal tensile stress and radial compressive or tensile stress. The mechanical damage would be more readily induced with the decrease of the spot size. Such a thermomechanical effect gives rise to the dependence of ablation depth and threshold fluence on laser spot size.

5. CONCLUSION

For the purpose of analyzing the mechanism of dependence of laser ablation depth and threshold fluence on laser spot size induced by ps laser pulses, a 2D asymmetric thermal mechanical model was developed and corresponding experimental cases were simulated. By analyzing the distribution of thermal stress in two directions, it has been found that the maximum longitudinal tensile stress at same time decreases and the corresponding coordinate shifts towards the surface as the spot size increases. Moreover since the radial tensile stress in each case is approximately only half the corresponding longitudinal one, the tensile stress along normal direction is the dominating force causing the deformation

of the material. The simulation qualitatively predicts the same trend of ablation depth as the experimental one in terms of laser induced thermal stress.

Furthermore, utilizing thermoelasticity theory the gradient of lattice temperature might be the dominant factor that has a detrminant impact on the value and distribution of the corresponding thermal stress. As lager gradients of lattice temperature can be obtained in smaller spot size cases with identical laser fluence, larger tensile stress is induced and this leads to a decreasing threshold fluence.

At last it should be noted that this model is plausible in the situation where the laser fluence is in the proximity of the melting threshold. The model predicts for copper a melting threshold fluence of approximately 2.5J/cm^2 in which case the maximum lattice temperature (1687K) is larger than the melting point copper (1357K). Once the target is melted hydrodynamic effects such as marangoni effect and surface tension should be taken into consideration for the molten layer, as the propagation of the stress wave could be different from that in solid state. Therefore such thermomechanical model is more suitable for cold ablation. For the case of higher laser fluences thermal ablation should be studied carefully. Further developments of this 2D model will probably consider such spot size dependent effects from the perspective of electron dynamics and hydrodynamics.

6. ACKNOWLEDGEMENTS

The author would like to thank the Know-how and Technology Transfer department of the Bern University of Applied Science for its financial support.

REFERENCES

[1] Benjamin Lauer, Beat Jaeggi, Yiming Zhang, Beat Neuenschwander, “Measurement of the maximum specific removal rate: unexpected influence of the experimental method and the spot size,” ICALE, Paper M701 (2015).

[2] Yu. V. Afanasiev, B. N. Chichkov, V. A. Isakov, A. P. Kanavin, and S. A. Uryupin, “Thermal regime of laser ablation of metals by ultrashort pulses of low fluence,” Journal of Russian Laser Research 20 (3), 189-201 (1999).

[3] B. Y. Mueller and B. Rethfeld, “Relaxation dynamics in laser-excited metals under nonequilibrium conditions,” Physical Review B 87, 035139 (2013).

[4] B. Neuenschwander, B. Jaeggi, M. Schmid, A. Dommann, A. Neels, T. Bandi, G. Hennig, “Factors controlling the incubation in the application of ps laser pulses on copper and iron surfaces,” Proc. of SPIE Vol. 8607, 86070D (2013).

[5] Zhigui Ou, Min Huang, and Fuli Zha, “Colorizing pure copper surface by ultrafast laser-induced near-subwavelength ripples,” Optics Express, 22(14), 17254-17265 (2014).

[6] R.F.W. Herrmann, J. Gerlach, E. E. B. Campbell, “Ultrashort pulse laser ablation of silicon: an MD simulation study,” Appl. Phys. A, 66, 35–42 (1998).

[7] D. S. Ivanov and l. V. Zhigilei, “Combined atomistic-continuum model for simulation of laser interaction with metals: application in the calculation of melting thresholds in Ni targets of varying thickness,” Appl. Phys. A, 79, 977–981 (2004).

[8] D. S. Ivanov, E. Yakovlev, V. P. Lipp, B. Rethfeld, V. P. Veiko, M. E. Garcia, "Molecular dynamics study of the short laser pulse ablation: quality and efficiency in production," Appl. Phys. A, 81(5), (2014).

[9] Robert A. Mitchell, Douglass Schumacher, Enam Chowdhury, "Using Particle-In-Cell simulations to model femtosecond pulse laser damage," Proc. of SPIE Vol. 9237, 92370X (2014).

[10] Ling Zhou and Ling Li, "Melting and resolidification of gold film irradiated by laser pulses less than 100 fs," Appl. Phys. A, 1-9 (2014).

[11] J.K. Chen , D.Y. Tzou , J.E. Beraun, "A semiclassical two temperature model for ultrafast laser heating, " International Journal of Heat and Mass Transfer, 49, 307–316 (2006) .

[12] J.K. Chen, J.E. Beraun , L.E. Grimes, D.Y. Tzou, "Modeling of femtosecond laser-induced non-equilibrium deformation in metal films," International Journal of Solids and Structures, 39, 3199–3216 (2002).

[13] Yong Gan, Yaogen Shen, Zhen Chen, "Reduction of the effect of electron relaxation behavior on the femtosecond laser-induced response of copper thin film by ballistic energy transfer," International Journal of Thermal Sciences, 93, 21-28 (2015).

[14] S.Y. Wang, Y. Ren, C.W. Cheng, J.K. Chen, D.Y. Tzou, "Micromachining of copper by femtosecond laser pulses," Applied Surface Science, 265, 302–308 (2013).

[15] Y. Zhang and J. K. Chen, "Melting and resolidification of gold film irradiated by nano- to femtosecond lasers," Appl. Phys. A, 88, 289–297 (2007).

[16] Carsten Schaefer, Herbert M. Urbassek and Leonid V. Zhigilei, "Metal ablation by picosecond laser pulses: A hybrid simulation," PHYSICAL REVIEW B, 66, 115404 (2002).

[17] J. Yang, Y. Zhao and X. Zhu, "Theoretical studies of ultrafast ablation of metal targets dominated by phase explosion," Appl. Phys. A, 89, 571–578 (2007).

[18] Carsten Schaefer, Herbert M. Urbassek and Leonid V. Zhigilei, "Metal ablation by picosecond laser pulses: A hybrid simulation," PHYSICAL REVIEW B, 66, 115404 (2002).

[19] T. Balasubramani and S. H. Jeong, "Simulation of the thermionic emission during ultrashort pulse laser ablation of metals," Journal of Physics: Conference Series, 59, 595–599 (2007).

[20] B.H. Christensen, K. Vestentoft, P. Balling, "Short-pulse ablation rates and the two-temperature model," Applied Surface Science, 253, 6347–6352 (2007).

[21] Sergei I. Anisimov , Baerbel Rethfeld, "Theory of ultrashort laser pulse interaction with a metal," Proc. SPIE 3093, Nonresonant Laser-Matter Interaction (NLMI-9), 192 (1997).

[22] Y. Jee, M.F. Becker and R.M. Walser, "Laser-induced damage on single-crystal metal surfaces," J. Opt. Soc. Am. B5, (1988).